Comparison, with an Analytical Optimization Process, of Two Synchronous Halbach Permanent Magnet Machines, for a Direct Drive Stick Application

Jean-Francois Allias[2, *], Jean-Francois Llibre[1], Carole Henaux[1], Yves Briere[2], and Soheib Fergani[2]

Abstract—This paper deals with the comparison of two actuators with different frameworks, for a direct drive active stick application. Each actuator will be compared with three different sets of specifications which impose many constraints as: high torque, small volume, low temperature, etc. The high required torque per unit of mass and the small volume allowed involve the use of synchronous Halbach permanent magnet (PM) topologies which have the best torque performances. In this article, an analysis and a comparison of two optimized actuators designed with a Halbach configuration are done. It is a linear actuator and a double airgap rotating actuator. The electromagnetic torque is calculated by the Laplace force for which the flux density generated by the Halbach PM configuration is defined by a Laplace equation and a Poisson equation. An analytical optimization under a set of nonlinear constraints will be realized with the analytical expressions of the torque we got previously. In order to validate the analytical model, finite-element analysis (FEA) simulations will be performed on the optimized structure. Finally, two actuators will be compared in order to give the best compromises for the stick application for each set of specifications.

1. INTRODUCTION

Most current aircraft use fly by wire with passive sticks to create force feedback. This force depends on the displacement angle of the stick compared to the natural resting position. Two passive sticks in the cockpit, on the left side for the pilot and on the right side for the co-pilot, create feedback forces by compression of springs. It has been demonstrated in [1–3] that active stick technology can improve haptics sensations in comparison with passive solution. Most of the time, the actuated sticks are made of a conventional rotating motor with a reducer. The requirements given by the aeronautical companies are highly restrictive: a high continuous torque per unit of mass (around 3.5 $(\mathrm{Nm{\cdot}Kg^{-1}})$), a low volume allocated, a low electric consumption and a low failure rate. Complying with all of these requirements is very difficult, and there are currently very few industrial active devices.

Three different sets of specifications will be studied. Each of them is linked with a different kind of aircraft. The first one is for a helicopter application (set 1), the second one for a small airplane (set 2) and the third one for a large airplane (set 3). For these applications, two structures are offered. The first one is a linear actuator called tubular Moving Magnet Actuator (MMA). It presents all the characteristics of a synchronous permanent magnet (PM) machine as in [4–6]. Figure 1 shows, for one axis (pitch or roll), the MMA structure. In the tubular MMA, the translator is composed of PM with a Halbach magnetization (as in [7]), fixed to a tubular magnetic circuit. This structure is an evolution

* Corresponding author: Jean-Francois Allias (jean-francois.allias@isae-supaero.fr).
[1] INPT, UPS; CNRS LAPLACE (Laboratoire PLAsma et Conversion d'Energie); ENSEEIHT, 2 rue Charles Camichel, BP 7122, F-31071, Toulouse Cedex 7, France. [2] ISAE (Institut Superieur de l'Aeronautique et de l'Espace), Departement DCAS, 31055 Toulouse, France.

of the structure presented in [8] where the PMs are only magnetized radially. This change improves the power density and therefore the expected performances of the actuator, as demonstrated in [9]. The second structure is a Double Airgap Rotating synchronous PM Machine with a non-entire arc called DARM, as in [10]. Figure 2 shows the DARM, for one axis (pitch or roll). In this rotating actuator, the rotors are also composed of PM with a Halbach magnetization, and the stator is composed of ring-shaped coils wounded on a yoke.

In scientific literature as in [1, 3, 11–13], the analytical models for the calculation of the magnetic flux density and the electromagnetic forces or torque are based on the Poisson equation, where the magnetization waveform created by PM is developed in Fourier series. That is the method which will be used in order to get a continuous function of the polarization of the magnets and to calculate the magnetic vector potential. As the ring-shaped coils are assembled without teeth and slots, the force (for the MMA) and torque (for the DARM) will be calculated by using the Laplace force as in [12].

Then, a process of optimization, under a set of nonlinear constraints, as the overall dimensions or the magnetic saturation is used in order to reach one of the best compromises for each structure and for each set of specifications.

In the second section of this paper, the set of specifications will be presented. In the third section, the models of the two actuators will be developed. In the fourth section, an optimization process is undertaken to determine the design parameters of the structures. In the fifth section, the theoretical results will be compared with the FEA results obtained with the Ansys software. Finally, the last sections present conclusions and acknowledgments.

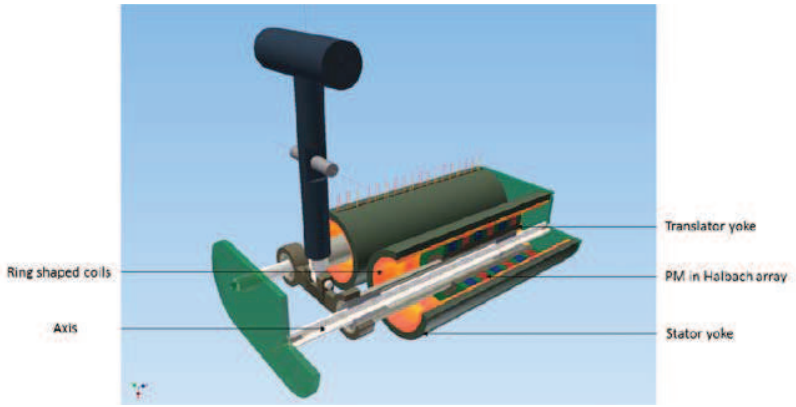

Figure 1. Tubular moving magnet actuator (MMA).

2. SET OF SPECIFICATIONS

Considering the specifications, the design must take into account a set of constraints such as available space, redundancy, stroke, speed, forces and torque ripples constraints. The application requires that the system must be redundant for each axis (pitch and roll). Thus, two actuators are implemented in parallel and are embedded in a box. Moreover, in case of power loss (the actuators are then ineffective), a passive solution with springs and dampers (or PM and copper such as in [14, 15]) has to be implemented. The passive solution is not studied in this paper. This architecture is called triplex.

The pilot, by hand operating the stick, applies a force F_p at the grip middle point distance d_{gmp} of the pivot point as in Figure 3.

Each part of the triplex (actuator or passive solution) has to develop a third of the force F_p. Then, the torque to be developed by each actuator can be expressed as following:

$$C_p = F_p \cdot d_{gmp} = 3.F_{act} \cdot R_{lever} = 3 \cdot C_{act} \tag{1}$$

In a passive stick, the effort is a linear function of the displacement angle. In the active technology, the force versus the displacement angle is not continuous, as illustrated in Figure 4.

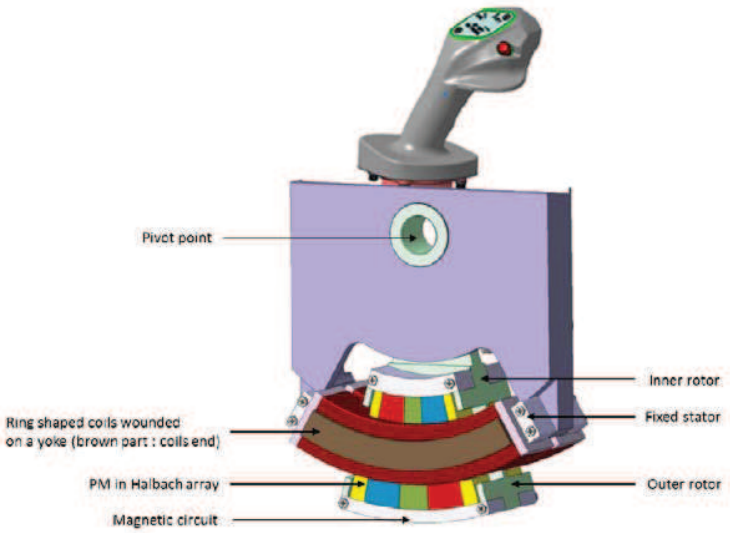

Figure 2. Double airgap rotative machine (DARM).

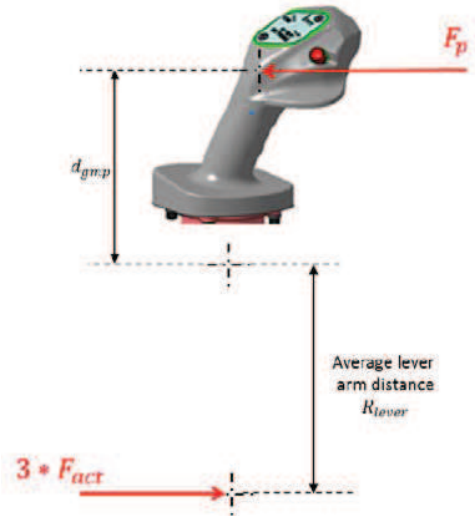

Figure 3. Grip middle point distance and average lever arm distance.

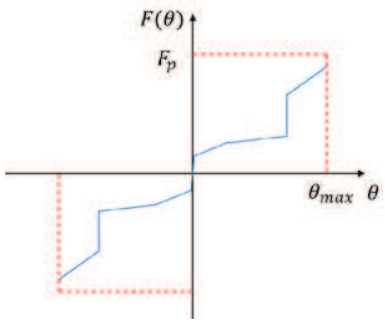

Figure 4. Force characteristic in function of the position.

Actually, the actuators have to develop a force for which the characteristic of effort compared to the position must be comprised onto the red dotted lines. The base point of the design is chosen on the maximal required force. From now, throughout the paper, F_p will be considered as the design point which corresponds to the maximal required force that the triplex must develop. Nevertheless, regarding the slope of the curve in Figure 4, even if it may be very high, most of the time, the pilot maintains the stick in his hand in a given position. It means that the dynamic of the side stick is quasi-static. Then, a sudden elevation of the force or the torque (F_m or C_m) produced by the actuator, as illustrated in Figure 4, does not imply a fast variation of the stick, because the pilot counters the effort produced by the actuator in his hand. Then, there is no reason that steep slope involves the production of huge mechanical stresses or discomfort of the passengers.

There are three different sets of specifications called set 1, set 2 and set 3. For each of them, the maximal required effort (or torque) to produce and the allocated parallelepiped boxes volume are different. Table 1 gives the volume of the embedded boxes, the torque or force to reach and the full range of movement ($[-\theta_{\max}; \theta_{\max}]$).

Table 1. Details of the three sets of specifications.

	Set 1	Set 2	Set 3
C_{act} (Nm)	3.2	12	14
F_{act} (daN)	2	7.2	8.5
Size box ($H_{box} \cdot L_{box} \cdot P_{box}$ (mm^3))	$150 \cdot 150 \cdot 60$	$220 \cdot 272 \cdot 120$	$304 \cdot 304 \cdot 165$
Full range of movement in (°)	$[-15; 15]$	$[-18; 18]$	$[-20; 20]$

For the predesign and optimization design, it is necessary to take into account the available space. Figure 5 and Figure 6 show the actuators in there own available space. The z axis is chosen in the direction of P_{box}, which is the lowest length value of the box.

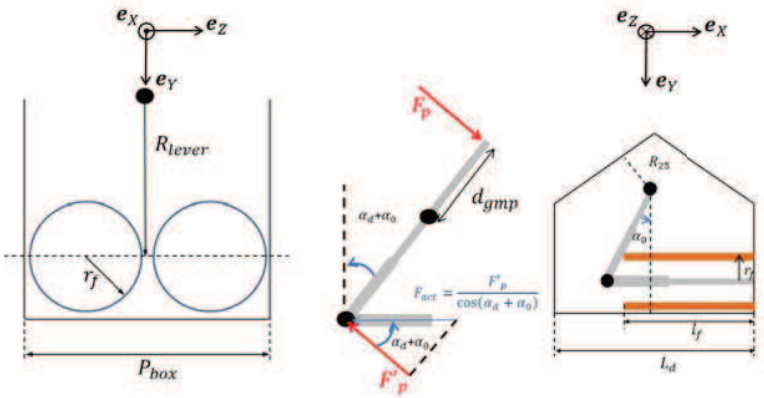

Figure 5. Overall dimensions of the MMA in the box.

From these figures, analytical formulations of such constraints can be expressed. Here, we just give some expressions of the constraints in relation with r_f, but we have at least 3 overall dimensions constraints in each direction for each actuator.

In the linear case:

$$4 \cdot r_f \leq P_{box} \tag{2}$$

And in the rotative case:

$$r_f \leq H_{box} \tag{3}$$

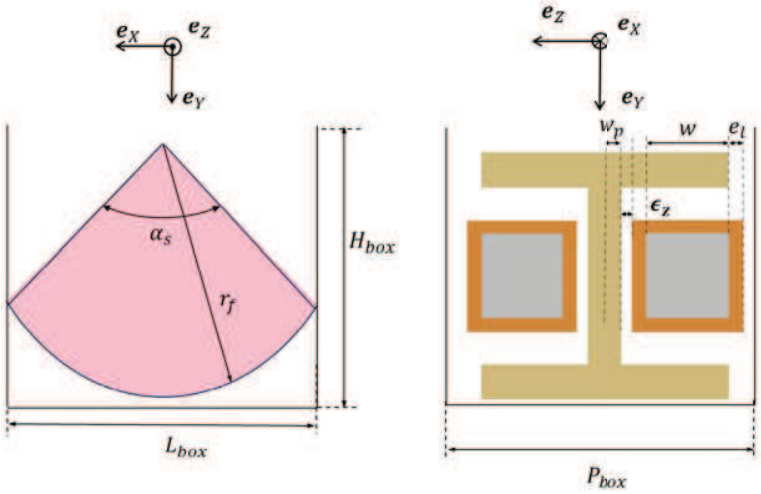

Figure 6. Overall dimensions of the DARM in the box.

3. PREDESIGN

Two different actuators will be compared. The first one called MMA, illustrated in Figures 1 and 5, is a linear tubular synchronous PM machine as in [11]. The ring-shaped coils supplied by a three-phase sinusoidal current system are molded and tied to the stator at the ends. The stator has no teeth in order to reduce the saliency effect. The ring-shaped PMs are mounted in a Halbach configuration.

The second actuator, called DARM, is a rotating synchronous PM machine with two airgaps illustrated in Figures 2 and 6. The ferromagnetic stator yoke is surrounded by the coils which are supplied by a three-phase sinusoidal current system. The inner and outer rotors are fixed by a plate and are composed of two iron yokes. The PMs are arranged in a Halbach array pattern.

The aim of this part is to develop a model which could be used for both structures, in order to optimize and compare it. Nevertheless, the frame of each actuator is very different, and the models should be different too. Indeed, the most appropriate model of the MMA is 2D axisymmetric, and the most appropriate model of the DARM is 3D in a cylindrical coordinate system. However, the conditions for neglecting edge effects and thus to develop a 2D model are not respected here. By this condition we mean that for the DARM $r_f < w$, with w illustrated in Figure 6 and, for the MMA $r_f < l_f$, with l_f illustrated in Figure 5, which is not the case. However, a 3D cylindrical model is too complex, and we want to develop 2D models. In order to try to keep out the flux lines in a 2D plane, we used a very high permeability iron cobalt and a Halbach array pattern of magnets. So, in this paper, we simulated the actuators in 2D. We could have done 3D FEA analysis in order to validate our choice but we built a prototype of the DARM. This prototype has been tested in [15]. It permits to validate the models.

The appropriate coordinate system of the MMA is Cartesian and cylindrical for the DARM. For both structures we give the same names to the units vector, which are (e_X, e_Y, e_Z). Anyway, for the MMA the coordinate system is fixed while the DARM one is a rotating reference frame.

In another way, any point M located on the cross sectional view will be characterized by the same X, Y variables. X, Y will represent the distances in m for the MMA and respectively the angle and radius for the DARM. X_R describes the rotor displacement. X_S describes the stator coils location, and X_{RS} describes the position of the rotor compared to the stator:

$$X_s = X_R + X_{RS} \tag{4}$$

There are two different cylindrical coordinates systems for both actuators. Figure 7 shows the coordinates systems for the linear actuator and for the rotative machine with a non-entire arc.

For the linear machine:

$$X_R = z_R, \quad Y = r, \quad X_{RS} = v \cdot t \tag{5}$$

For the rotative machine:

$$X_R = \theta_R, \quad Y = r, \quad X_{RS} = \Omega \cdot t \tag{6}$$

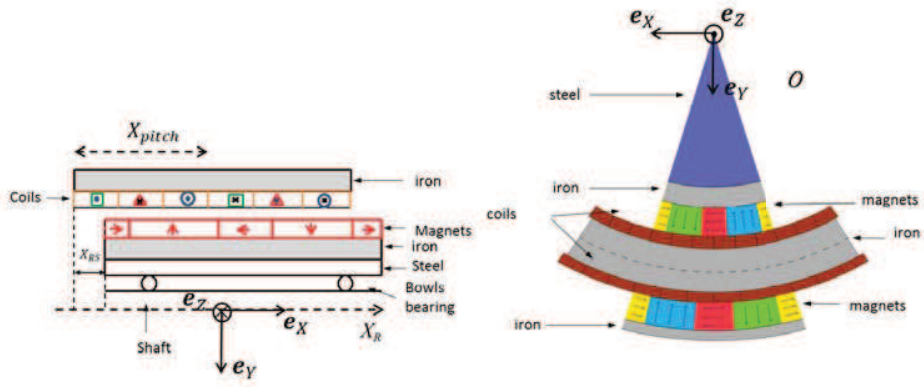

Figure 7. Coordinates systems for both structures.

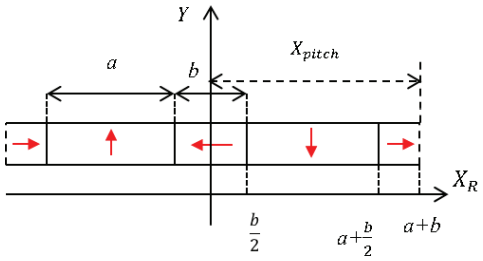

Figure 8. Halbach array pattern.

where v is the linear speed in m/s and Ω is the rotation speed in rad/s.

An important remark is that for the DARM, two different actuators are considered which are delimited by the black dotted line in Figure 7. Above, it is the internal machine and below, it is the external machine. The internal and the external torques are added in order to get the total torque produce by the actuator. Because of the high required torque per unit of mass, a Halbach array magnetization of the PM is used. Figure 8 shows an illustration of a pole pair pattern (which comprises a combination between radial and ortho-radial magnetization), where X_{pitch} is the length of a half pole pair of magnets. The Halbach array allows to shrink the rotor iron yoke because the magnetic flux density is more concentrated in the airgap than in the rotor yoke.

In order to design the Halbach pattern of magnets, the parameter λ is defined as:

$$\lambda = \frac{b}{X_{pitch}} \tag{7}$$

Actually, λ is the ratio between the tangential magnetization over the pole pitch.

In order to calculate the magnetic flux density in the airgap, taking into account the Halbach magnetization, a model with the vector potential $\mathbf{A}$ is used, and it is defined as:

$$\mathbf{B} = \nabla \times \mathbf{A} \tag{8}$$

where $\mathbf{B}$ is the magnetic flux density and $\nabla\times$ the curl vector operator. The study domain is separated into three areas respectively named A_i, A_m and A_a (iron Area, magnet Area and airgap Area) as represented in Figure 9.

In the aim of getting a fast result, the hypothesis that the iron permeability is infinite is made. After developing the Maxwell's equations, the following expressions are obtained as in [7, 11]:

$$\begin{aligned} \mathbf{\Delta A} &= 0 \quad (A_a) \\ \mathbf{\Delta A} &= -\mu_0 \nabla \times \mathbf{M} \quad (A_m) \end{aligned} \tag{9}$$

where $\mathbf{M}$ is the remanent magnetization, μ_0 the vacuum permeability and $\mathbf{\Delta}$ the Laplacian vector operator.

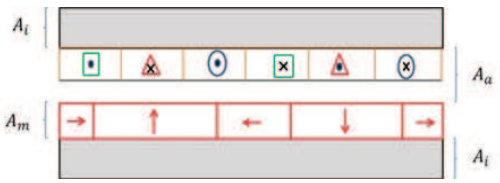

Figure 9. Magnetic's areas.

The classic way to solve the Laplace and Poisson equations is to develop the remanent magnetization in Fourier series. $\mathbf{M}$ is a vector, and a projection on the X_R and Y axis is realized:

$$\mathbf{M} = M_{X_R}(X_R)\mathbf{e}_X + M_Y(X_R)\mathbf{e}_Y \tag{10}$$

Finally, the expressions of the projected remanent magnetization are:

$$\begin{aligned} M_{X_r}(X_R) &= \sum_{n=1}^{+\infty} M_{nX_R}(X_R)\cos(nK \cdot X_R) \\ M_Y(X_R) &= \sum_{n=1}^{+\infty} M_{nY}(X_R)\sin(nK \cdot X_R) \end{aligned} \tag{11}$$

where M_{nX_R} and M_{nY} are the Fourier coefficients which depend on the kind of magnetization. Their expressions are different when the magnetization is parallel or radial [16].

After calculating the vector potential $\mathbf{A}$, the magnetic flux densities are obtained thanks to Eq. (8) as in [11]. The magnetic flux density is $\mathbf{B}^{(A_a)}$ in the magnetic airgap and $\mathbf{B}^{(A_m)}$ in the magnets. Only the radial part B_Y creates a force feedback. The expressions of B_Y are given respectively in Eqs. (12) and (13) in the (A_a) and (A_m) areas, for the MMA and the DARM.

$$\begin{aligned} B_Y^{(A_a)}(X_R,Y) &= \sum_{n=1}^{+\infty}(\zeta_{1n}^a \cdot \cosh(nK \cdot Y) + \zeta_{2n}^a \cdot \sinh(nK \cdot Y)) \cdot (\zeta_{3n}^a \cdot \cos(nK \cdot X_R) + \zeta_{4n}^a \cdot \sin(nK \cdot X_R)) \\ B_Y^{(A_m)}(X_R,Y) &= \sum_{n=1}^{+\infty}(\zeta_{1n}^m \cdot \cosh(nK \cdot Y) + \zeta_{2n}^m \cdot \sinh(nK \cdot Y) + \beta_n(Y)) \cdot (\zeta_{3n}^m \cdot \cos(nK \cdot X_R) + \zeta_{4n}^m \cdot \sin(nK \cdot X_R)) \end{aligned} \tag{12}$$

$$\begin{aligned} B_Y^{(A_a)}(X_R,Y) &= \sum_{n=1}^{+\infty}(\zeta_{1n}^{'a} \cdot Y^{nK} + \zeta_{2n}^{'a} \cdot Y^{-nK}) \cdot (\zeta_{3n}^{'a} \cdot \cos(nK \cdot X_R) + \zeta_{4n}^{'a} \cdot \sin(nK \cdot X_R)) \\ B_Y^{(A_m)}(X_R,Y) &= \sum_{n=1}^{+\infty}(\zeta_{1n}^{'m} \cdot Y^{nK} + \zeta_{2n}^{'m} \cdot Y^{-nK} + \beta_n(Y)) \cdot (\zeta_{3n}^{'m} \cdot \cos(nK \cdot X_R) + \zeta_{4n}^{'m} \cdot \sin(nK \cdot X_R)) \end{aligned} \tag{13}$$

$K = \frac{\pi}{X_{pitch}}$ is a parameter in rad/m which allows to convert the distance in an angle for the MMA. For the DARM (rotative case), it represents the number of poles of an entire arc machine: K has no units.

β is a function calculated with the help of the Poisson equation given in Equation (9) and which satisfies Equation (14). ζa_{in}, ζm_{in}, $\zeta' a_{in}$ and $\zeta_{in}^{'m}$, for $i = 1, \ldots, 4$, are constants calculated with the interface conditions.

$$\sum_{n=1}^{+\infty} \beta_n(Y) \cdot (\zeta_{3n}^{'m} \cdot \cos(nK \cdot X_R) + \zeta_{4n}^{'m} \cdot \sin(nK \cdot X_R)) = -\mu_0 \nabla \times \mathbf{M} \tag{14}$$

Then the Laplace force (or torque) is calculated thanks to Eq. (15).

$$\begin{aligned} \mathbf{dF}_L &= I \cdot \mathbf{dl} \times \mathbf{B} \\ \mathbf{dC}_L &= Y \cdot \mathbf{e}_Y \times \mathbf{dF}_L = r\mathbf{e}_r \times \mathbf{dF}_L \end{aligned} \tag{15}$$

The actuator is supplied by a three phases sinusoidal currents system. Considering the synchronism condition required to provide a non zero average force or torque, the supplying current is a space-time function given in Eq. (16). $I_c^k(t)$ may be defined as shown in Figure 10.

$$I_c^k(t) = \hat{I} \cdot \sin\left(\omega_s \cdot t + \frac{(k-1)\pi}{3} + \phi\right) \tag{16}$$

where ω_s is the pulsation of the currents, and $I_c^k(t)$ depends on the position of the coil compared to the stator with $k = \{1, 2, 3\}$. ϕ is the setting angle of the machine. $\hat{I}$ is determined taking into account the current density, $\hat{J}_c$ in A/mm^2 and the fill factor k_f. We have got:

$$\hat{I} = k_f \cdot \hat{J}_c \cdot S_{slot} \tag{17}$$

where S_{slot} is a coil area illustrated in Figure 10. Because of the geometry of the DARM, the fill factor is lower than in the MMA. For the DARM, $k_f = 0.54$, for the MMA, $k_f = 0.75$.

X_{wegde} is also defined, and it represents the width of the wedge between coils. Indeed, even if the actuators have no teeth, nonmagnetic wedges need to be put between the coils in order to insulate and to position each of them.

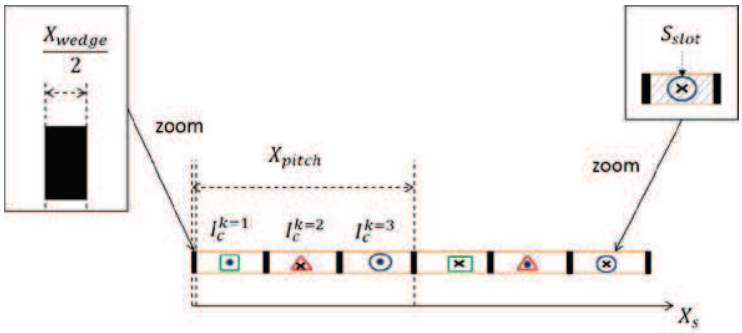

Figure 10. Space current repartition.

Finally, the total force (or the total torque) developed by each coil at the t instant has been expressed by calculating the average of the Laplace force (or Laplace torque) in Eq. (18) over a coil area named S_{slot}.

$$\begin{aligned} F_L^k(t) &= \frac{1}{S_{slot}} \int_{S_{slot}} \int_0^{2\pi} B_Y(X_S, Y, t) \cdot I_c^k(X_S, t) \cdot d\theta \cdot dS_{slot} \\ C_L^k(t) &= \frac{1}{S_{slot}} \int_{S_{slot}} \int_z Y \cdot B_Y(X_S, Y, t) \cdot I_c^k(X_S, t) \cdot dz \cdot dS_{slot} \end{aligned} \tag{18}$$

In order to get the total force of the linear actuator or the total torque of the rotating machine, we consider a three-phase sinusoidal current, and the results are given by:

$$\begin{aligned} F_m(t) &= 2p \sum_{k=1}^{3} F_L^k(t) \\ C_m(t) &= 2p \sum_{k=1}^{3} C_L^k(t) \end{aligned} \tag{19}$$

Where p is the number of pairs of poles.

4. OPTIMIZATION

Like any aeronautical embedded system, the sets of specifications are very strict about dimensional and heating constraints for our actuator. But, it has to provide a high torque in a small volume. So, in

order to reach a point which can satisfy all these constraints, a multi-objective function with nonlinear equality and inequality constraints has been created, as in [17].

$$\begin{aligned} &\min_{\mathbf{x}\in\Omega} f \\ &g_i(\mathbf{x}) \leq 0,\ \forall i \in (1,\ldots,n_g) \\ &h_j(\mathbf{x}) = 0,\ \forall j \in (1,\ldots,n_h) \end{aligned} \tag{20}$$

where f is the objective function to minimize, and g_i and h_i are respectively the functions which represent the inequality constraints and equality constraints. n_g and n_h represent respectively the number of inequality and equality equations. For the MMA $\mathbf{x} \in \mathbb{R}^{10}$ and for the DARM $\mathbf{x} \in \mathbb{R}^{13}$, where $\mathbf{x}$ is the vector of the variables of the optimization problem.

The function f can be developed as the following expression:

$$f(\mathbf{x}) = \sum_i \gamma_i \frac{f_i(\mathbf{x})}{|f(\mathbf{x})|} \tag{21}$$

with:

$$\sum_i \gamma_i = 1 \tag{22}$$

where f_i is each mono-objective function, and γ_i is the weight given to each objective. Here, there are two main objectives which are the force (or the torque) and the Joule losses called P_{joule}. In the linear case $f_1 = -F_m(t)$ and in the rotative case $f_1 = -C_m(t)$, where F_m and C_m are the force and torque values for the maximum allowed current to be compare with the maximum torque $C_{act} = \frac{C_p}{3}$ or effort $F_{act} = \frac{F_p}{3}$ to reach. The second objective is, in both cases, equal to the Joule losses: $f_2 = P_{joule}$. The mechanical power is, in the linear case:

$$P_m = F_m \cdot v \tag{23}$$

And in the rotative case:

$$P_m = C_m \cdot \Omega \tag{24}$$

and,

$$P_{joule} = 3.R_{copper}.I_{RMS}^2 \tag{25}$$

As a low speed application, the maximum frequency is around 3 Hz. So, the iron losses are neglected, and the efficiency of both actuators, called η, is given by Eq. (26).

$$\eta = \frac{P_m}{P_m + P_{joule}} \tag{26}$$

In order to realize this optimization, the TOOLBOX OPTIMIZATION of MATLAB has been used. The minimization function "$fmincon$" and the "Interior-point" algorithm as in [18] have been chosen. The "global-search" function which is based on a multi-start method has also been used. Indeed, each departure point of the optimization process, except the first one which is imposed by the user, is chosen by an internal algorithm. The final result is the best local minimum reached with all these departure points.

Table 2 and Table 3 show respectively the results of the optimizations for the linear actuator and for the rotative actuator, for the three sets of specifications and for five different couples of weights (γ_1, γ_2). In Table 2 and Table 3 the authors give for each optimization, the torque C_m to be compared to $C_{act} = \frac{C_p}{3}$ from Table 1, the Joule losses P_{joule} and the efficiency η in %. For the linear actuator, the equivalent torque is equal to $R_{lever} \cdot F_m(t)$, where R_{lever} is the distance of the average lever arm as illustrated in Figures 3 and 5.

The constraints of the optimizations are based on the overall dimensions, the magnetic saturation of the iron yokes, the mass, and the torque to reach. The equalities constraints are more difficult to satisfy and take more CPU time. That is why we impose inequality constraints such as $C_{act} \leq C_m(t) \leq 1.02C_{act}$. It means that, if there is a value upper than C_{act} in the table, the process has succeeded, and the actuator reaches a torque which complies with the set. The mass and magnetic saturation are also in agreement with the set of specifications. If the actuator is unable to satisfy the set of specifications,

Table 2. Results of the multi-objectives optimizations for the three sets of specifications for the MMA.

Linear actuator	Set 1: $C_{act} = 3.2$ (Nm)			Set 2: $C_{act} = 12$ (Nm)			Set 3: $C_{act} = 14$ (Nm)		
Exit parameters	C_m (Nm)	P_{joule} (W)	η	C_m	P_{joule}	η	C_m	P_{joule}	η
$(\gamma_1, \gamma_2) = (1, 0)$	0.81	3.3	30.0% (NF)	39.03	176.9	27.8%	53.41	98.6	48.6%
$(\gamma_1, \gamma_2) = (\frac{2}{3}, \frac{1}{3})$	0.78	3.13	30.3% (NF)	36.01	153.9	29.0%	52.33	95.8	48.8%
$(\gamma_1, \gamma_2) = (\frac{1}{2}, \frac{1}{2})$	0.65	2.5	31.2% (NF)	20.89	81.1	31.0%	37.11	93.2	41%
$(\gamma_1, \gamma_2) = (\frac{1}{3}, \frac{2}{3})$	0.54	2	31.9.0% (NF)	15.30	41.6	39.1%	14.10	30.6	44.56%
$(\gamma_1, \gamma_2) = (0, 1)$	0.51	1.9	32.1% (NF)	12.02	32.1	39.5%	14.00	29.9	45%

Table 3. Results of the multi-objectives optimizations for the three sets of specifications for the DARM.

Rotative actuator	Set 1: $C_{act} = 3.2$ (Nm)			Set 2: $C_{act} = 12$ (Nm)			Set 3: $C_{act} = 14$ (Nm)		
Exit parameters	C_m	P_{joule}	η	C_m	P_{joule}	η	C_m	P_{joule}	η
$(\gamma_1, \gamma_2) = (1, 0)$	3.96	42.45	14.0%	38.03	119	35.8%	44.28	115.9	40.0%
$(\gamma_1, \gamma_2) = (\frac{2}{3}, \frac{1}{3})$	3.70	32	16.8%	33.43	113.3	34%	36.80	96.3	40.0%
$(\gamma_1, \gamma_2) = (\frac{1}{2}, \frac{1}{2})$	3.30	27.9	17.1%	29.84	96.7	35.0%	27.03	57.4	45.1%
$(\gamma_1, \gamma_2) = (\frac{1}{3}, \frac{2}{3})$	3.13	24.9	18.0% (NF)	12.05	12.4	62.8%	14.46	24.9	50.3%
$(\gamma_1, \gamma_2) = (0, 1)$	2.97	21.4	19.5% (NF)	12.00	11.9	63.7%	14	19	56.3%

then the torque, Joule losses and efficiency are also given, but the mention NF (Not Feasible) is written in the tables.

For the MMA in Table 2, set 1 is too restrictive. There is no solution (NF) because $C_m < C_{act}$ (Nm). For sets 2 and 3, there are solutions for all the couples of (γ_1, γ_2). However, for the couple of weights $(\gamma_1, \gamma_2) = (0, 1)$, the optimization tends to minimize the joule losses (and so the efficiency). In the opposite, for the couple of weights $(\gamma_1, \gamma_2) = (1, 0)$, the torque is maximized, then the joule losses are huge, and the efficiency is low. For the DARM in Table 3, the same remarks may be made. Finally, for each set of specifications, the DARM seems to be the actuator which reaches the best compromise between torque and efficiency. For example, if we watch the last lines of both Tables 2 and 3 (which are linked to the couple of weights $(\gamma_1, \gamma_2) = (0, 1)$) for the sets 2 and 3, the efficiencies are respectively 39.5% and 45% for the MMA and 63.7% and 56.3% for the DARM. Nevertheless, if we watch the third line of both tables for sets 2 and 3 (and most particularly for the set 3), which refers to $(\gamma_1, \gamma_2) = (1, 0)$, the MMA seems to be able to produce more torque (in a short time).

5. ANALYTICAL AND FINITE ELEMENT SIMULATION RESULTS

The finite element simulation has been performed with the Ansys software in quasi-static conditions. It is here $2D$ simulations with triangular meshing. Both frameworks are simulated in the $(\mathbf{e}_X, \mathbf{e}_Y)$ plan from Figure 7 with an axisymmetric boundary condition for the linear structure. The region around the actuators is in air, and the boundary conditions are zero vector potential.

Figure 11 shows the flux lines created by the Halbach array PM patterns without load. We can notice that the rotor or translator iron yokes are less saturated than the stator yokes, because a part of the flux lines are swallowed by the ortho-radially magnetized magnets. The effort or torque, developed with load, has been calculated with the help of the virtual work and Maxwell stress tensor methods.

Many FEA simulations have been performed in the aim of validating the results of Table 2 and Table 3. To avoid making the paper unwieldy, the authors will just show the results obtained from two structures which respect sets 1 and 2. It means that just the FEA simulations performed for the rotative framework in the set 1 for the couple of weights $\gamma = (\frac{1}{2}, \frac{1}{2})$, and the simulations performed for the linear structure in set 2 for the couple of weights $\gamma = (0, 1)$ will be shown.

Table 4 gives the results obtained by the Ansys software for the DARM with the following values of $\gamma = (\frac{1}{2}, \frac{1}{2})$.

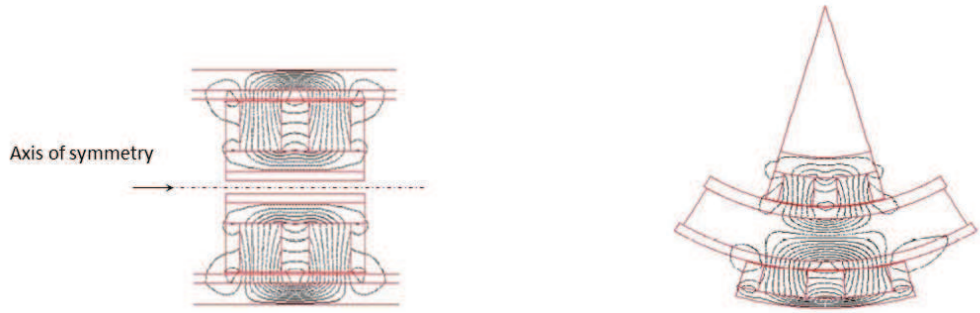

Figure 11. Flux lines of both structures simulated.

Table 4. Results of the quasi-static simulation performed with the Ansys Software for the DARM.

	Analytical model in (19)	Ansys software simulation	
Rotative actuator set 1	Analytical torque	Maxwell stress tensor	Virtual Works
C_m (Nm)	3.30	3.32	3.33

Table 5 gives the results obtained by the Ansys software for the MMA with the following values of $\gamma = (0, 1)$.

Table 5. Results of the quasi-static simulation performed with the Ansys Software for the MMA.

	Analytical model in (19)	Ansys software simulation	
Linear actuator set 2	Analytical force	Maxwell stress tensor	Virtual Works
F_m (N)	63.9	64.3	64.2
$C_m = R_{lever} * F_m$ (Nm)	12.02	12.08	12.07

It might be interesting to show the waveform created by PMs calculated by ANSYS, with no load, in the airgap, and to compare it with the analytical expression obtained thanks to Eq. (13). Figure 12 illustrates the waveform created by the Halbach pattern of PMs of the external airgap of the DARM.

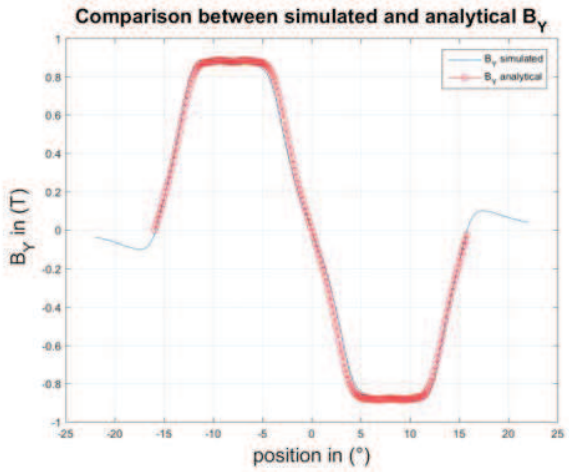

Figure 12. Comparison between the simulated and analytical waveform created by the Halbach array pattern of PMs with no load in the external airgap of the DARM.

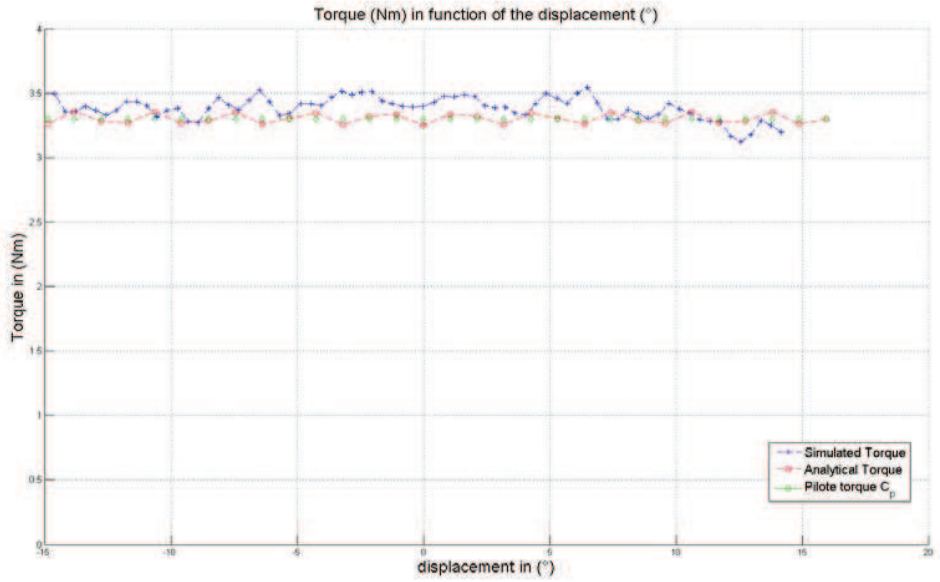

Figure 13. Comparison of the evolution of the simulated and analytical torque in a full range of movement of the DARM which respects the set 1.

The evolution of the simulated torque in function of the displacement of the rotor is given in Figure 13, in a full range of movement of $[-15°; +15°]$ from set 1, for the DARM. It is compared with the analytical torque given by Eq. (19).

The results between the two FEA simulations methods given in Table 5 are close, which means that the meshing is well done. It is also close to the theoretical torque results. The authors are now able to compare the two frameworks in order to make the best choice.

6. CONCLUSIONS

When Tables 2 and 3 are observed, it is difficult to point out which one is the best structure. The results highly depend on the set of specifications, and most particularly on the allocated volume. Indeed, on a closer examination of Equation (2) and Figures 5 and 7, it is possible to see that the shaft and bowls bearing of the MMA, which have a constant size, take too much space for set 1. It is the reason that the MMA does not reach the torque C_{act} on the second column of the Table 2.

However, for set 3, the torque reached for the couple of weights (1, 0) is higher with the MMA than the DARM. There are two main reasons to explain this fact. The first one is that the repartition of the magnets in front of the coils is better for the MMA. The second one is that the fill factor of the coils of the MMA is better than the one with the DARM.

In this paper, two topologies of direct drive actuated sticks for an aeronautical application have been presented. The calculation of the force and the torque developed by each actuator is based on an analytical approach. With the help of FEA simulations, the analytical calculations have been verified for optimized structures. The authors finally give the advantages and disadvantages of each framework in order to be able to choose the best one for each set of specifications.

ACKNOWLEDGMENT

This paper has been supported by the French Research National Agency within the framework of the program ANR-12-INSE-0006. This program is labelled by the Aerospace Valley, pole of competitiveness in aeronautics, space and embedded systems of Aquitaine and Midi-Pyrenees Regions in south of France.

REFERENCES

1. Hosman, R. J., B. Bernard, and H. Fourquet, "Active and passive side stick controllers in manual aircraft control," *Systems, Man and Cybernetics*, 1990.
2. Hanke, D. and C. Herbst, "Active sidestick technology: A means for improving situational awareness," *Aerospace Science and Technology*, Vol. 3, 1999.
3. Hegg, J. W., M. P. Smith, L. Yount, and J. Todd, "Features of active sidestick controllers," *IEEE Aerospace and Electronics Systems Magazine*, Vol. 7, 1995.
4. Jang, S. M., J. Y. Choi, S. H. Lee, H. W. Cho, and W. B. Jang, "Analysis and experimental verification of moving-magnet linear actuator with cylindrical Halbach array," *IEEE Trans. on Magnetics*, Vol. 40, No. 4, 2068–2070, 2004.
5. Ben Ahmed, H., B. Multon, and M. Ruellan, "Actionneurs lineaires directs et indirects," *revue3EI*, 38–58, 2004.
6. Amara, Y. and G. Barakat, "Analytical modeling of magnetic field in surface mounted permanent magnet tubular linear machines," *IEEE Trans. on Magnetics*, Vol. 46, No. 11, 3870–3884, 2010.
7. Yan, L., L. Zhang, J. Y. Wang, Z. Jiao, C. Y. Chen, and I. M. Chen, "Magnetic field of tubular linear machines with dual Halbach array," *Progress In Electromagnetic Research*, Vol. 136, 283–299, 2013.
8. Allias, J. F., J. F. Llibre, C. Henaux, Y. Briere, and D. Alazard, "A global approach for the study of forces developed by a tubular liear moving magnet actuator," *XXI International Conference on Electrical Machines ICEM*, 2014.
9. Allias, J. F., J. F. Llibre, D. Harribey, C. Henaux, and D. Alazard, "Approche globale de l etude des efforts developpes par un actionneur MMA tubulaire," *Symposium de Genie Electrique SGE*, 2014.
10. Mohammadi, S. and M. Mirsalim, "Analytical design framework for torque and back-EMF optimization, and inductance calculation in double-rotor radial-flux air-cored permanent-magnet synchronous machine," *IEEE Trans. on Magnetics*, Vol. 50, No. 1, 2014.
11. Chikouche, B. L., K. Boughrara, and R. Ibtiouen, "Cogging torque minimization of surface-mounted permanent magnet synchronous machines using hybrid magnet shapes," *Progress In Electromagnetic Research*, Vol. 62, 49–61, 2015.
12. Bianchi, N., "Analytical computation of magnetic fields and thrusts in a tubular PM linear servo motor," *IEEE Industry Application Conference*, Vol. 1, 21–28, Rome Italy, 2000.
13. Trumper, D. L., W. J. Kim, and M. E. Williams, "Design and analysis framework for linear permanent magnet machines," *IEEE Trans. on Industry Applications*, Vol. 32, No. 2, 1996.
14. Harribey, D., J. F. Allias, J. F. Llibre, and C. Henaux, "Dispositif de commande passif magnetique," *Patent*, WO2015150439A2, 2015
15. Allias, J. F., "Dimensionnement d un actionneur pour organe de pilotage a entrainement direct avec redondance passive magnetique," *These de l Institut National Polytechnique de Toulouse*, 2015
16. Dubas, F., C. Espanet, and A. Miraoui, "Modelisation analytique et maximisation de l'induction magnetique a vide d'un moteur a aimants montes en surface," *Electrotechnique du Futur*, 2003.
17. Fitan, E., F. Messine, and B. Nogarede, "The electromagnetic actuator design problem: A general and rational approach," *IEEE Trans. on Magnetics*, Vol. 40, No. 3, 2004.
18. Naimi, D. and T. Bouktir, "Optimal power flow using interior point method," *International Conference on Electrical Engineering Design and Technologies*, Hammamet, Tunisia, 2007.